Model for quantitative analysis of reflection-electron-energy-loss spectra: Angular dependence

F. Yubero
Laboratoire pour l'Utilisation du Rayonnement Electromagnétique, Bâtiment 209d, Centre Universitaire Paris-Sud, F-91405 Orsay, France

J. M. Sanz
Instituto Universitario Nicolás Cabrera and Departamento de Física Aplicada C-XII, Universidad Autónoma de Madrid, Cantoblanco, E-28049 Madrid, Spain

B. Ramskov and S. Tougaard
Department of Physics, University of Odense, DK-5230 Odense M, Denmark
(Received 14 August 1995)

A model to reproduce inelastic electron scattering cross sections as determined from reflection-electron-energy-loss experiments is proposed. This model is an extension of model B from Yubero and Tougaard [Phys. Rev. B **46**, 2486 (1992)]. Here, a more general geometry is considered where the incidence and exit angles can be varied. Then, for a given geometry and energy of the primary electrons, the dielectric function of the sample is the only input for the calculations. A systematic study of the behavior of the model is presented for the case of Si and Fe.

I. INTRODUCTION

Quantification of electron spectroscopies as x-ray photoelectron spectroscopy, Auger electron spectroscopy, REELS (reflection-electron-energy-loss spectroscopy), or x-ray absorption spectroscopy rely on a thorough understanding of the energy losses of electrons as they travel within the surface region (up to 100 Å depth) of solids. Therefore, the study of the inelastic scattering properties of low-energy electrons (100–10 000 eV) is very important for these surface electron spectroscopies.

The inelastic electron scattering cross section describes the energy losses of electrons traveling in solids. In principle, this function depends on the energy of the electron interacting with the solid, its trajectory, and the dielectric properties of the medium considered.

It is well known[1,2] that the inelastic scattering cross section $K_{\rm bulk}(E_0,\hbar\omega)$ for electrons traveling in an infinite medium is given by

$$K_{\rm bulk}(E_0,\hbar\omega)=\frac{1}{\pi E_0 a_0}\int_{k_-}^{k_+}\frac{dk}{k}\,{\rm Im}\left\{\frac{1}{\epsilon(k,\omega)}\right\},$$

where E_0, $\hbar\omega$, and k are the kinetic energy, the energy loss, and the momentum transferred by the electron, respectively, $k_\pm=(2m/\hbar^2)^{1/2}[E_0^{1/2}\pm(E_0-\hbar\omega)^{1/2}]$ are the maximum and minimum momentum transfer allowed by the energy and momentum conservation laws, a_0 is the Bohr radius, and ϵ the dielectric function of the medium. For small values of k, the dependence of ϵ on k is weak compared with $1/k$, so the general shape of $K_{\rm bulk}(E_0,\hbar\omega)$ is given as a first approximation by the energy-loss function (ELF) ${\rm Im}\{1/\epsilon(\omega)\}$. Then, the ELF governs the energy losses of electrons traveling in the bulk of a solid.

If we consider an electron traveling through a thin foil,[2–5] it is found that the corresponding inelastic scattering cross section $K_{\rm foil}(E_0,\hbar\omega,b,\alpha)$ is given by

$$K_{\rm foil}(E_0,\hbar\omega,b,\alpha)=K_{\rm bulk}(E_0,\hbar\omega)+K_{\text{surf-foil}}(E_0,\hbar\omega,b,\alpha),$$

where in general $K_{\text{surf-foil}}(E_0,\hbar\omega,b,\alpha)$ is a complicated function of ϵ, the foil thickness b, and the angle of incidence α of the primary electrons with respect to the surface normal of the foil. $K_{\text{surf-foil}}(E_0,\hbar\omega,b,\alpha)$ gives the surface contribution to the total energy losses of the electrons. These surface excitations are produced within a few angstroms of the total thickness of the foil localized at the two interfaces of the foil with the vacuum. The size of this ''surface region'' has a physical extension that increases with the square root of the energy E_0 of the electrons.[2,5] It comes out that, for large enough thicknesses, the surface energy-loss function ${\rm Im}\{1/(\epsilon+1)\}$ governs the inelastic cross section $K_{\text{surf-foil}}(E_0,\hbar\omega,b,\alpha)$.

The interpretation of inelastic electron scattering cross sections obtained from REELS experiments appears more complicated than the situations described above. The electrons follow many different trajectories inside the solid within its surface region, and all of them contribute to the measured cross section. Many authors[6] have considered that the combined effect of the surface and bulk excitations can be modeled by a linear combination of ${\rm Im}\{1/\epsilon\}$ and ${\rm Im}\{1/(\epsilon+1)\}$. Although reproducing the shape of experimental cross sections with this approximation is possible, the fitting parameters carry limited quantitative information.[7]

In Ref. 8 a model was considered where it is assumed that the surface energy losses in a REELS experiment can be obtained from the surface energy losses calculated for a transmission geometry when the thickness of the foil is large enough that the surface losses have reached their saturation value.[2–5] The validity of this approximation is ques-

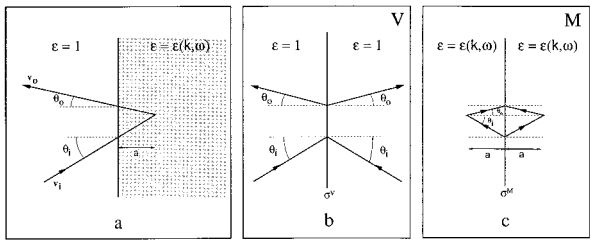

FIG. 1. Trajectory followed by the electron in a REELS experiment (a) and the equivalent pseudomedia V (b) and M (c), which has been used in the present formalism to evaluate $K_{\rm eff}$ (see text).

tionable because the major part of the electrons that contribute to the spectral intensity in the energy region of interest have traveled a path length less than ~ 2 inelastic mean free paths (IMFP). Thus, the surface term in Refs. 2, 3 varies considerably for values of a up to ~ 2 IMFP's. In practice, the surface term reaches its saturation for $b > 20E_0^{1/2}/\hbar\omega$ (where $\hbar\omega$ and E_0 given in eV, and a given in Å), which for the losses of interest (up to ~ 100 eV) corresponds to path lengths larger than 1–2 IMFP. Furthermore, the geometry of the REELS experiment is different from the transmission experiment, and it is not clear that the surface energy losses measured in an electron reflection experiment will be well reproduced by those calculated for electrons transmitted through a thin film.

A more realistic model was developed to describe the electron energy losses in REELS experiments.[9] It is based on a quantitative description of the energy losses of electrons traveling in a certain REELS geometry (normal incidence of the incoming electrons and specular reflection by an elastic scattering event). It takes into account the depth dependence of the effective inelastic scattering cross section. The formalism allows one to obtain information about dielectric properties of solids as well as to estimate the IMFP. During the last years it has been successfully applied to several materials[10,11] (Si, SiO_2, ZrO_2).

In this work we present an extension of that model to treat a more general geometry in which both the angle of incidence and exit angle for the electrons can be varied arbitrarily. The only restriction is that both trajectories must lie in the same plane normal to the surface.

The present formalism is based on the so-called ''surface reflection model.''[12,13] This model has been quite useful for applications in studies of particle-surface interaction processes, and in calculations of the energy loss of particles reflected or moving in the proximity of a solid surface.[13,14] The approach allows one to derive the various interference terms that influence the electron energy dissipation. In the frame of the proposed new formalism, model B in Ref. 9 appears as a particular case for a given geometry.

II. THEORY

We study the problem of an electron traveling in a REELS geometry, as shown in Fig. 1(a). An incident electron travels in vacuum toward a solid with a velocity $\mathbf{v}_i=(v_{\perp i}, v_{\parallel i})$, where $v_{\perp i}=v\cos\theta_i$ and $v_{\parallel i}=v\sin\theta_i$ are, respectively, the components perpendicular and parallel to the surface, and θ_i is the angle of incidence measured with respect to the surface normal. At $t=-a/v_{\perp i}$ it enters the solid characterized by its dielectric function $\epsilon(\mathbf{k},\omega)$. At the point $\mathbf{a}=(a,0)$ inside the solid at $t=0$, it is elastically backscatered. Then, it changes direction and it leaves the solid with a velocity $\mathbf{v}_o=(-v_{\perp o}, v_{\parallel o})$, where $v_{\perp o}=v\cos\theta_o$ and $v_{\parallel o}=v\sin\theta_o$ are, respectively, the components perpendicular and parallel to the surface, and θ_o is the exit angle. It is assumed that the energy lost by the electron $\hbar\omega$ is much smaller than the primary energy of the electron $E_0=\frac{1}{2}mv^2$, so $|\mathbf{v}_i|=|\mathbf{v}_o|$.

We want to calculate the inelastic electron single scattering cross section to be compared with the cross section measured experimentally in a REELS experiment. To do that, we first have to obtain an expression for the effective inelastic electron scattering cross section $K_{\rm eff}(E_0,\hbar\omega,a,\theta_i,\theta_o)$. This is defined as the average probability that the electron shall lose energy $\hbar\omega$ per unit energy loss and per unit path length when traveling in the trajectory described in Fig. 1(a). The average is taken over the total path length $x=a(1/\cos\theta_i+1/\cos\theta_o)$ traveled by the electron in the solid. Then, the experimental REELS cross section is a ''weighted average'' of $K_{\rm eff}(E_0,\hbar\omega,a,\theta_i,\theta_o)$ for different values of a (see below).

It is found that $K_{\rm eff}(E_0,\hbar\omega,a,\theta_i,\theta_o)$ can be obtained from the expression[9]

$$K_{\rm eff}(E_0,\hbar\omega,a,\theta_i,\theta_o)=\mathrm{Re}\left\{\frac{-2i}{(2\pi)^4\hbar^2\omega x}\times\int d\mathbf{k}\int d\mathbf{r}\int dt\times e^{i(\mathbf{k}\cdot\mathbf{r}-\omega t)}\mathbf{k}\cdot\mathbf{v}\rho_e(\mathbf{r},t)\Phi_{\rm ind}(\mathbf{k},\omega)\right\},\tag{1}$$

where $\rho_e(\mathbf{r},t)$ is the charge density of the electron and $\Phi_{\rm ind}(\mathbf{k},\omega)=\Phi(\mathbf{k},\omega)-\Phi_{\rm vac}(\mathbf{k},\omega)$ is the potential induced by the electron in the full space [$\Phi(\mathbf{k},\omega)$ being the potential for the situation in Fig. 1(a) and $\Phi_{\rm vac}(\mathbf{k},\omega)$ is $\Phi(\mathbf{k},\omega)$ for $\epsilon=1$]. Then, the first step of our calculation of $K_{\rm eff}(E_0,\hbar\omega,a,\theta_i,\theta_o)$ is to obtain the potential $\Phi(\mathbf{k},\omega)$.

In this paper, the ''surface reflection model''[12,13] has been used to obtain $\Phi(\mathbf{k},\omega)$. It allows one to solve the problem of calculating the potential of a system of moving charges within a semi-infinite medium by considering two infinite pseudomedia (see Fig. 1). Then, to calculate the potential $\Phi(\mathbf{k},\omega)$ in the full Fourier space describing the situation of Fig. 1(a) two pseudomedia M [Fig. 1(c)] and V [Fig. 1(b)] are considered. The pseudomedium M is an infinite medium characterized by the dielectric function $\epsilon(\mathbf{k},\omega)$ with a surface charge density σ^M at $x=0$. In this pseudomedium we consider the electron and its image charge traveling while they are inside the medium in the real case [Fig. 1(a)] i.e., for times $-a/v_{\perp i}<t<a/v_{\perp o}$. The pseudomedium V is vacuum ($\epsilon=1$) with a surface charge density σ^V at $x=0$. Here we consider the electron and its image charge traveling while they are in vacuum in the real case, i.e., for times $t<-a/v_{\perp i}$ and $t>a/v_{\perp o}$. The scheme is illustrated in Fig. 1, which shows the real system [part (a)] and the equivalent pseudomedia V [part (b)] and M [part (c)]. The fictitious surface charges σ^M and σ^V are introduced to be able to fulfill the boundary conditions (see below).

The charge density $\rho_e(\mathbf{r},t)$ describing the trajectory in the real space of the electron and its image charge $\rho_{e'}(\mathbf{r},t)$ are given by

$$\rho_e(\mathbf{r},t)=\begin{cases}-e\,\delta(\mathbf{r}-\mathbf{a}-\mathbf{v}_i t), & \text{if } t<0\\ -e\,\delta(\mathbf{r}-\mathbf{a}-\mathbf{v}_o t), & \text{if } t>0,\end{cases} \tag{2}$$

$$\rho_{e'}(\mathbf{r},t)=\begin{cases}-e\,\delta(\mathbf{r}-\mathbf{a}'-\mathbf{v}_i' t), & \text{if } t<0\\ -e\,\delta(\mathbf{r}-\mathbf{a}'-\mathbf{v}_o' t), & \text{if } t>0,\end{cases} \tag{3}$$

where $\mathbf{v}_i'=(-v_{\perp i}v_{\parallel i})$, $\mathbf{v}_o'=(v_{\perp o},v_{\parallel o})$, and $\mathbf{a}'=(-a,0)$ are the velocity of the incident image charge, the velocity of the exit image charge, and the point where it is backscattered, respectively.

According to the surface reflection model,[12,13] the potential $\Phi(\mathbf{k},\omega)$ in Fourier space is given by $\Phi^M(\mathbf{k},\omega)$ while the electron is traveling in the medium $(-a/v_{\perp i}<t<a/v_{\perp o})$ and by $\Phi^V(\mathbf{k},\omega)$ while the electron is traveling in vacuum ($t<-a/v_{\perp i}$ and $t>a/v_{\perp o}$). Then, the pseudomedia M and V have been introduced to evaluate the pseudopotentials Φ^M and Φ^V. The Poisson equations of the two pseudomedia in Fourier space are

$$\Phi^V(\mathbf{k},\omega)=\frac{4\pi}{k^2}\,[\rho^V(\mathbf{k},\omega)+\sigma^V(k_\parallel,\omega)], \tag{4}$$

$$\Phi^M(\mathbf{k},\omega)=\frac{4\pi}{\epsilon(\mathbf{k},\omega)k^2}\,[\rho^M(\mathbf{k},\omega)+\sigma^M(k_\parallel,\omega)]. \tag{5}$$

Here, $\rho^V(\mathbf{k},\omega)$ and $\rho^M(\mathbf{k},\omega)$ are the Fourier transforms of the pseudo charge densities in each pseudomedium, and they are given by

$$\rho^V(\mathbf{k},\omega)=\int_{-\infty}^{-a/v_{\perp i}}dt\;e^{i\omega t}\int d\mathbf{r}\;e^{-i\mathbf{k}\cdot\mathbf{r}}[\rho_e(\mathbf{r},t)+\rho_{e'}(\mathbf{r},t)]+\int_{a/v_{\perp o}}^{\infty}dt\;e^{i\omega t}\int d\mathbf{r}\;e^{-i\mathbf{k}\cdot\mathbf{r}}[\rho_e(\mathbf{r},t)+\rho_{e'}(\mathbf{r},t)], \tag{6}$$

$$\rho^M(\mathbf{k},\omega)=\int_{-a/v_{\perp i}}^{a/v_{\perp o}}dt\;e^{i\omega t}\int d\mathbf{r}\;e^{-i\mathbf{k}\cdot\mathbf{r}}[\rho_e(\mathbf{r},t)+\rho_{e'}(\mathbf{r},t)]. \tag{7}$$

The pseudo-surface-densities $\sigma^V(k_\parallel,\omega)$ and $\sigma^M(k_\parallel,\omega)$ are determined by the requirement that the pseudopotentials Φ^V and Φ^M and the normal components of the displacement vectors D_n^V and D_n^M of each pseudomedia have to be continuous at $x=0$, i.e., $\Phi^V(x=0)=\Phi^M(x=0)$ and $D_n^V(x=0)=D_n^M(x=0)$. From this it follows that $\sigma^V(k_\parallel,\omega)=-\sigma^M(k_\parallel,\omega)=\sigma(k_\parallel,\omega)$ where

$$\sigma(k_\parallel,\omega)=\frac{k_\parallel}{\pi}\left[1+\frac{k_\parallel}{\pi}\int\frac{dk_\perp}{k^2\epsilon(\mathbf{k},\omega)}\right]^{-1}\int_{-\infty}^{\infty}\frac{dk_\perp}{k^2}\left[\frac{\rho^M(\mathbf{k},\omega)}{\epsilon}-\rho^V(\mathbf{k},\omega)\right]=\frac{k_\parallel}{\pi}\frac{\epsilon}{\epsilon+1}\int_{-\infty}^{\infty}\frac{dk_\perp}{k^2}\left[\frac{\rho^M(\mathbf{k},\omega)}{\epsilon}-\rho^V(\mathbf{k},\omega)\right]. \tag{8}$$

To obtain the last expression, it has been assumed that either $\epsilon(\mathbf{k},\omega)=\epsilon(k_\parallel,\omega)$ or $\epsilon(\mathbf{k},\omega)=\epsilon(\omega)$. Although the validity of this approximation is not clear, it is needed to obtain an analytical expression. The same approximation was made in the formalism for the thin foil transmission geometry[2,3] and in Ref. 9. The approximation may be justified because of the weak dependence of ϵ on $\mathbf{k}$ compared with the rest of the terms in the integrals.[9]

From Eqs. (2)–(8), it is straightforward to find the induced potentials $[\Phi_{\rm ind}^{M,V}(\mathbf{k},\omega,\epsilon)=\Phi^{M,V}(\mathbf{k},\omega,\epsilon)-\Phi^{M,V}(\mathbf{k},\omega,\epsilon=1)]$

$$\Phi_{\rm ind}^M(\mathbf{k},\omega)=\frac{4\pi}{k^2}\,\rho^M(\mathbf{k},\omega)\left\{\frac{1}{\epsilon}-1\right\}+\frac{4\pi}{k^2}\,F^{MM}(k_\parallel)\,\frac{(\epsilon+2)(\epsilon-1)}{\epsilon(\epsilon+1)}-\frac{4\pi}{k^2}\,F^{MV}(k_\parallel)\,\frac{(\epsilon-1)}{(\epsilon+1)}, \tag{9}$$

$$\Phi_{\rm ind}^V(\mathbf{k},\omega)=-\frac{4\pi}{k^2}\,[F^{MM}(k_\parallel)+F^{MV}(k_\parallel)]\,\frac{(\epsilon-1)}{(\epsilon+1)}, \tag{10}$$

where

$$\rho^M(\mathbf{k},\omega)=\rho_1^M(\mathbf{k},\omega)+\rho_2^M(\mathbf{k},\omega), \tag{11}$$

$$\rho_1^M(\mathbf{k},\omega)=\frac{ie}{v_{\perp i}}\left[\frac{-e^{-i\Omega_i a}}{\Omega_i-k_\perp}\right]+\frac{ie}{v_{\perp o}}\left[\frac{e^{i\Omega_o a}}{\Omega_o+k_\perp}\right]+\frac{ie}{v_{\perp i}}\left[\frac{e^{ik_\perp a}-e^{-i\Omega_i a}}{\Omega_i+k_\perp}\right]-\frac{ie}{v_{\perp o}}\left[\frac{e^{ik_\perp a}-e^{i\Omega_o a}}{\Omega_o-k_\perp}\right], \tag{12}$$

$$\rho_2^M(\mathbf{k},\omega)=\frac{ie}{v_{\perp i}}\left[\frac{e^{-ik_\perp a}}{\Omega_i-k_\perp}\right]-\frac{ie}{v_{\perp o}}\left[\frac{e^{-ik_\perp a}}{\Omega_o+k_\perp}\right], \tag{13}$$

$$F^{MM}(k_\parallel)=\frac{k_\parallel}{2\pi}\int_{-\infty}^{+\infty}\frac{dk_\perp}{k^2}\,\rho^M(\mathbf{k},\omega)=\frac{ie}{v_{\perp i}}\left[\frac{e^{-k_\parallel a}-e^{-i\Omega_i a}}{\Omega_i+ik_\parallel}\right]-\frac{ie}{v_{\perp o}}\left[\frac{e^{-ik_\parallel a}-e^{i\Omega_o a}}{\Omega_o-ik_\parallel}\right], \tag{14}$$

$$F^{MV}(k_\parallel)=\frac{k_\parallel}{2\pi}\int_{-\infty}^{+\infty}\frac{dk_\perp}{k^2}\,\rho^V(\mathbf{k},\omega)=\frac{ie}{v_{\perp i}}\left[\frac{e^{-i\Omega_i a}}{\Omega_i-ik_\parallel}\right]-\frac{ie}{v_{\perp o}}\left[\frac{e^{i\Omega_o a}}{\Omega_o+ik_\parallel}\right], \tag{15}$$

with $\Omega_{i,o}=(\omega-k_\parallel v_{\parallel i,o})/v_{\perp i,o}$.

Now, Eqs. (2) and (9)–(15) can be introduced in Eq. (1) to obtain $K_{\rm eff}(E_0,\hbar\omega,a,\theta_i,\theta_o)$. We have to perform first the integrals in space and time. In doing this, we have to take into account that we have a different expression for the pseudopotentials Φ^M and Φ^V depending on where the electron at a given time is located in real space (see Fig. 1). Then, the effective inelastic scattering cross section can be expressed as the sum of four contributions, which correspond to the losses of the electron while traveling in vacuum $K_{\rm eff}^{V_i}$ and in the medium $K_{\rm eff}^{M_i}$ for the incoming trajectory and in vacuum $K_{\rm eff}^{V_o}$ and in the medium $K_{\rm eff}^{M_o}$ for the exit trajectory,

$$K_{\rm eff}=K_{\rm eff}^{V_i}+K_{\rm eff}^{M_i}+K_{\rm eff}^{M_o}+K_{\rm eff}^{V_o}. \tag{16}$$

Each term can be found from the following expressions:

$$K_{\rm eff}^{V_i}=\mathrm{Re}\left\{\frac{2ie}{(2\pi)^4\hbar^2\omega x}\int d\mathbf{k}\left(k_\perp+k_\parallel\frac{v_{\parallel i}}{v_{\perp i}}\right)e^{ik_\perp a}\Phi_{\rm ind}^V(\mathbf{k},\omega)\left[\pi\delta(k_\perp-\Omega_i)-i\,\frac{e^{-i(k_\perp-\Omega_i)a}}{k_\perp-\Omega_i}\right]\right\},\tag{17}$$

$$K_{\rm eff}^{M_i}=\mathrm{Re}\left\{\frac{-2e}{(2\pi)^4\hbar^2\omega x}\int d\mathbf{k}\left(k_\perp+k_\parallel\frac{v_{\parallel i}}{v_{\perp i}}\right)e^{ik_\perp a}\Phi_{\rm ind}^M(\mathbf{k},\omega)\left[\frac{1-e^{-i(k_\perp-\Omega_i)a}}{k_\perp-\Omega_i}\right]\right\},\tag{18}$$

$$K_{\rm eff}^{V_o}=\mathrm{Re}\left\{\frac{-2ie}{(2\pi)^4\hbar^2\omega x}\int d\mathbf{k}\left(k_\perp-k_\parallel\frac{v_{\parallel o}}{v_{\perp o}}\right)e^{ik_\perp a}\Phi_{\rm ind}^V(\mathbf{k},\omega)\left[\pi\delta(k_\perp+\Omega_o)-i\,\frac{e^{-i(k_\perp+\Omega_o)a}}{k_\perp+\Omega_o}\right]\right\},\tag{19}$$

$$K_{\rm eff}^{M_o}=\mathrm{Re}\left\{\frac{2e}{(2\pi)^4\hbar^2\omega x}\int d\mathbf{k}\left(k_\perp-k_\parallel\frac{v_{\parallel o}}{v_{\perp o}}\right)e^{ik_\perp a}\Phi_{\rm ind}^M(\mathbf{k},\omega)\left[\frac{1-e^{-i(k_\perp+\Omega_o)a}}{k_\perp+\Omega_o}\right]\right\}.\tag{20}$$

Equations (16)–(20) give the solution to the problem of finding $K_{\rm eff}$ for a general REELS geometry. However, in the following we will consider approximations that allow some integrals to be done analytically.

The integrals in momentum are given by the conservation laws for energy and momentum. Unfortunately a complete analytical integration is not possible. However, with cylindrical coordinates ($d\mathbf{k}=2\pi dk_\parallel dk_\perp$) and extending the limits of integration over $k_\perp$ to $-\infty<k_\perp<+\infty$, the integral over $k_\perp$ can be done analytically. With this approximation we do not expect large errors because the main contribution to the integral comes from small values of k, and the integrand decreases roughly as $1/k^9$ for $k\to\pm\infty$ using the functional shape for the ELF as in Eq. (30) (see below). Assuming again $\epsilon=\epsilon(k_\parallel,\omega)$, it is found that

$$K_{\rm eff}^{V_i}=\mathrm{Re}\left\{\frac{e}{\hbar^2\omega\pi x}\frac{v_{\perp i}+iv_{\parallel i}}{v_{\perp i}}\int dk_\parallel\,\frac{\epsilon-1}{\epsilon+1}\frac{k_\parallel(k_\parallel+i\Omega_i)}{k_\parallel^2+\Omega_i^2}\,e^{i\Omega_i a}[F^{MM}(k_\parallel)+F^{MV}(k_\parallel)]\right\},\tag{21}$$

$$K_{\rm eff}^{V_o}=\mathrm{Re}\left\{\frac{-e}{\hbar^2\omega\pi x}\frac{v_{\perp o}-iv_{\parallel o}}{v_{\perp o}}\int dk_\parallel\,\frac{\epsilon-1}{\epsilon+1}\frac{k_\parallel(k_\parallel-i\Omega_o)}{k_\parallel^2+\Omega_o^2}\,e^{-i\Omega_o a}[F^{MM}(k_\parallel)+F^{MV}(k_\parallel)]\right\},\tag{22}$$

$$\begin{aligned}K_{\rm eff}^{M_i}=&\mathrm{Re}\left\{\frac{-2ie^2}{\hbar^2\pi v_{\perp i}^2}\frac{a}{x}\int dk_\parallel\left(\frac{1}{\epsilon}-1\right)\frac{k_\parallel}{k_\parallel^2+\Omega_i^2}\right\}+\mathrm{Re}\left\{\frac{-2e^2}{\hbar^2\pi v_{\perp o}\omega x}\int dk_\parallel\left(\frac{1}{\epsilon}-1\right)\frac{e^{i(\Omega_i+\Omega_o)}-1}{\Omega_i+\Omega_o}\frac{k_\parallel}{k_\parallel^2+\Omega_o^2}\left[k_\parallel\left(\frac{v_{\parallel i}}{v_{\perp i}}+\frac{v_{\parallel o}}{v_{\perp o}}\right)\right.\right.\\&\left.\left.-\frac{\omega}{v_{\perp o}}\right]\right\}+\mathrm{Re}\left\{\frac{e}{\hbar^2\pi\omega x}\frac{v_{\perp i}-iv_{\parallel i}}{v_{\perp i}}\int dk_\parallel\left(\frac{1}{\epsilon}-1\right)\frac{k_\parallel(k_\parallel-i\Omega_i)}{k_\parallel^2+\Omega_i^2}(e^{-k_\parallel a}-e^{i\Omega_i a})\rho_1^M(k_\perp=ik_\parallel)\right\}\\&+\mathrm{Re}\left\{\frac{e}{\hbar^2\pi\omega x}\frac{v_{\perp i}+iv_{\parallel i}}{v_{\perp i}}\int dk_\parallel\left(\frac{1}{\epsilon}-1\right)\frac{k_\parallel(k_\parallel+i\Omega_i)}{k_\parallel^2+\Omega_i^2}(e^{k_\parallel a}-e^{i\Omega_i a})\rho_2^M(k_\perp=-ik_\parallel)\right\}\\&+\mathrm{Re}\left\{\frac{e}{\hbar^2\pi^2\omega x}\frac{v_{\perp i}-iv_{\parallel i}}{2v_{\perp i}}\int dk_\parallel\left[\frac{(\epsilon+2)(\epsilon-1)}{\epsilon(\epsilon+1)}F^{MM}(k_\parallel)-\frac{\epsilon-1}{\epsilon+1}F^{MV}(k_\parallel)\right]\frac{k_\parallel(k_\parallel-i\Omega_i)}{k_\parallel^2+\Omega_i^2}(e^{-k_\parallel a}-e^{i\Omega_i a})\right\},\end{aligned}\tag{23}$$

$$\begin{aligned}K_{\rm eff}^{M_o}=&\mathrm{Re}\left\{\frac{-2ie^2}{\hbar^2\pi v_{\perp o}^2}\frac{a}{x}\int dk_\parallel\left(\frac{1}{\epsilon}-1\right)\frac{k_\parallel}{k_\parallel^2+\Omega_o^2}\right\}+\mathrm{Re}\left\{\frac{2e^2}{\hbar^2\pi v_{\perp i}\omega x}\int dk_\parallel\left(\frac{1}{\epsilon}-1\right)\frac{e^{-i(\Omega_i+\Omega_o)}-1}{\Omega_i+\Omega_o}\frac{k_\parallel}{k_\parallel^2+\Omega_i^2}\left[k_\parallel\left(\frac{v_{\parallel i}}{v_{\perp i}}+\frac{v_{\parallel o}}{v_{\perp o}}\right)\right.\right.\\&\left.\left.-\frac{\omega}{v_{\perp i}}\right]\right\}+\mathrm{Re}\left\{\frac{-e}{\hbar^2\pi\omega x}\frac{v_{\perp o}+iv_{\parallel o}}{v_{\perp o}}\int dk_\parallel\left(\frac{1}{\epsilon}-1\right)\frac{k_\parallel(k_\parallel+i\Omega_o)}{k_\parallel^2+\Omega_o^2}(e^{-k_\parallel a}-e^{-i\Omega_o a})\rho_1^M(k_\perp=ik_\parallel)\right\}\\&+\mathrm{Re}\left\{\frac{-e}{\hbar^2\pi\omega x}\frac{v_{\perp o}-iv_{\parallel o}}{v_{\perp o}}\int dk_\parallel\left(\frac{1}{\epsilon}-1\right)\frac{k_\parallel(k_\parallel-i\Omega_o)}{k_\parallel^2+\Omega_o^2}(e^{k_\parallel a}-e^{-i\Omega_o a})\rho_2^M(k_\perp=-ik_\parallel)\right\}\\&+\mathrm{Re}\left\{\frac{-e}{\hbar^2\pi^2\omega x}\frac{v_{\perp o}+iv_{\parallel o}}{2v_{\perp o}}\int dk_\parallel\left[\frac{(\epsilon+2)(\epsilon-1)}{\epsilon(\epsilon+1)}F^{MM}(k_\parallel)-\frac{\epsilon-1}{\epsilon+1}F^{MV}(k_\parallel)\right]\frac{k_\parallel(k_\parallel+i\Omega_o)}{k_\parallel^2+\Omega_o^2}(e^{-k_\parallel a}-e^{-i\Omega_o a})\right\}.\end{aligned}\tag{24}$$

Notice that $K_{\rm eff}^{V_o,M_o}$ can be obtained from $K_{\rm eff}^{V_iM_i}$ by making the changes $v_{\perp o}\to-v_{\perp i}$, $v_{\perp j}\to-v_{\perp o}$, $v_{\parallel i}\to v_{\parallel o}$, and $v_{\parallel o}\to v_{\parallel i}$. Note also that in general $K_{\rm eff}(E_0,\hbar\omega,a,\theta_o,\theta_o)\neq K_{\rm eff}(E_0,\hbar\omega,a,\theta_0,\theta_i)$, i.e., the losses experienced by the electron depend not only on the line trajectory followed but also on the sense in which it is done. However, in practice the difference is very small.

We must discuss now the limits in which the present model can be compared with model B in Ref. 9. That model is valid for normal incidence and exit angles of the electrons. This situation is given in the present model by considering $v_{\parallel i}=v_{\parallel o}=0$ and $v_{\perp i}=v_{\perp o}=v$, which gives

$$K_{\rm eff}(E_0,\hbar\omega,a,0,0)=\mathrm{Re}\left\{\frac{-2e^2i}{\hbar^2\pi v^2}\int dk_\parallel\left(\frac{1}{\epsilon}-1\right)\frac{k_\parallel}{k_\parallel^2+\Omega^2}\right\}+\mathrm{Re}\left(\frac{-4e^2i}{\hbar^2\pi v\omega 2a}\int dk_\parallel\frac{k_\parallel}{(k_\parallel^2+\Omega^2)^2}\left\{k_\parallel(e^{-k_\parallel a}-2\cos\Omega a)\right.\right.$$
$$\times(\Omega\cos\Omega a+k_\parallel\sin\Omega a)\frac{\epsilon-1}{\epsilon+1}+(\Omega^2+k_\parallel^2)\sin\Omega a\cos\Omega a\left(1-\frac{1}{\epsilon}\right)+(\Omega e^{k_\parallel a}-\Omega\cos\Omega a$$
$$\left.\left.+k_\parallel\sin\Omega a)\left[k_\parallel e^{k_\parallel a}\frac{(\epsilon-1)(\epsilon+2)}{\epsilon(\epsilon+1)}-2\Omega\sin\Omega a\left(1-\frac{1}{\epsilon}\right)-2k_\parallel\cos\Omega a\frac{(\epsilon-1)}{\epsilon(\epsilon+1)}\right]\right\}\right), \tag{25}$$

where $\Omega=\omega/v$.

This expression is identical to that of model B in Ref. 9 for the limits $a\to 0$ and $a\to\infty$. For other values of a they differ by less than 5%. This is clear from Fig. 2, where the results for the effective inelastic scattering cross section for Fe at 2000 eV are compared for two different paths traveled by the electron. This small deviation comes from the different mathematical model descriptions for the evaluation of the induced potentials used in the two models.

In the limit $a\to\infty$, only the first term in Eqs. (23) and (24) remains from the general expression for $K_{\rm eff}$ [i.e., Eq. (16)] and it can be shown that, as expected, for small incidence and exit angles this term equals the inelastic electron scattering cross section for electrons traveling in an infinite medium. However, for large incident and exit angles this is not the case. This is due to the approximations made in the model.

Until now, we have calculated analytical expressions for the effective inelastic scattering cross section $K_{\rm eff}(E_0,\hbar\omega,a,\theta_o,\theta_o)$ as a function of their primary energy E_0, the dielectric function of the system $\epsilon(\mathbf{k},\omega)$, the maximum depth a reached by the electron before being elastically backscattered, and the angles of incidence θ_i and exit θ_o of the electron trajectory. However, the cross section determined from an experimental REELS spectrum[15] has contributions from electrons that have reached different depths in the solid. To compare this cross section with theory, it is necessary to estimate the path-length distribution function Q for those electrons that have undergone a single inelastic scattering event.

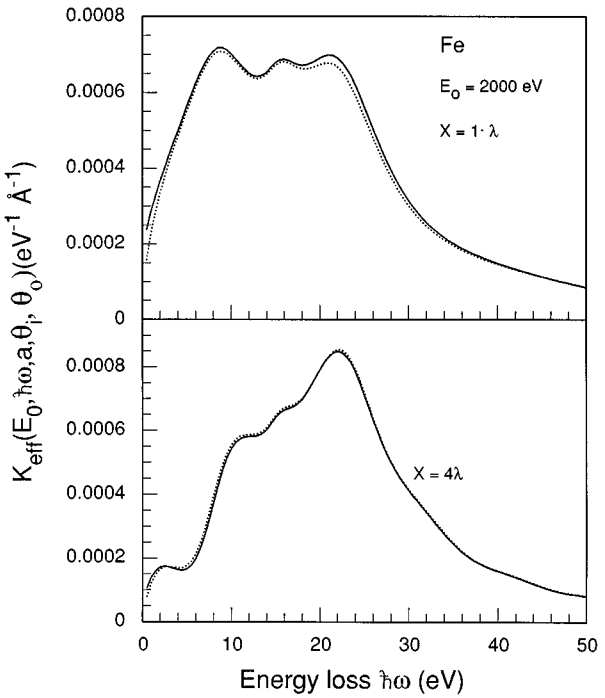

FIG. 2. Effective inelastic scattering cross section $K_{\rm eff}$ for Fe at 2000 eV calculated according to model *B* in Ref. 9 (points) and in this work by Eq. (25) (full line) for two path lengths ($x=\lambda$ and 4λ with $\lambda=27.7$ Å) traveled by the electron. The dielectric function for Fe was taken from Ref. 20.

Small-angle elastic scattering is highly favored but this does not affect the trajectory significantly. The transport mean free path for elastic scattering is much larger than the inelastic mean free path.[16] Therefore, most of the REELS electrons in the energy range of interest have undergone a single large-angle scattering event. Then, for a fixed incidence θ_i and θ_o angles, the contribution to the measured inelastic scattering cross section $K_{\rm sc}(E_0,\hbar\omega,\theta_i,\theta_o)$ is a weighted average over the total path length x of $K_{\rm eff}(E_0,\hbar\omega,a,\theta_i,\theta_o)$ with the weight function given by $Q(E_0,x,\theta_i,\theta_o)$ as

$$K_{\rm sc}(E_0,\hbar\omega,\theta_i,\theta_o)=\frac{\int_0^\infty dx Q(E_0,x,\theta_i,\theta_o)K_{\rm eff}(E_0,\hbar\omega,a,\theta_i,\theta_o)}{\int_0^\infty dx Q(E_0,x,\theta_p,\theta_o)}. \tag{26}$$

The path-length distribution function for all the electrons measured in a REELS experiment is, to a good approximation, given by[15] $e^{-x/L}$ where the characteristic length $L\gg\lambda$.[16,17] Q in Eq. (26) is the path-length distribution function for those REELS electrons that have undergone a single inelastic loss. If we assume that the inelastic events are independent, the scattering probability along the path traveled by the electron will be given by a Poisson distribution, then the probability that one electron has had only one inelastic scattering is $(x/\lambda)e^{-x/\lambda}$. Q is therefore $(x/\lambda)e^{-x/\lambda}e^{-x/L}$.

In general, the inelastic mean free path $\lambda(E_0)$ is related to the inelastic electron scattering cross section by

$$\lambda(E_0)=\left[\int_0^\infty d\hbar\omega K(E_0,\hbar\omega)\right]^{-1}. \tag{27}$$

We can define the effective inelastic mean free path $\lambda_{\rm eff}(E_0,a,\theta_i,\theta_o)$ for electrons traveling in the geometry described in Fig. 1(a) as

$$[\lambda_{\rm eff}(E_0,a,\theta_i,\theta_o)]^{-1}=\int_0^{E_{\rm max}} d\hbar\omega K_{\rm eff}(E_0,\hbar\omega,a,\theta_i,\theta_o) + [\lambda_c(E_0)]^{-1}, \tag{28}$$

where $E_{\rm max}$ is the maximum energy $\hbar\omega$ available for $K_{\rm eff}$ and λ_c accounts for the scattering contribution of the core levels at binding energies above $E_{\rm max}$.[18] For a typical case with $E_{\rm max}\approx 100$ eV, the correction introduced by λ_c in $\lambda_{\rm eff}$ is below 10%.

Then, the inelastic scattering cross section determined from REELS can be written as Eq. (26) with $Q(E_0,x,\theta_i,\theta_o)$ given by

$$Q(E_0,x,\theta_i,\theta_o)=\frac{x}{\lambda_{\rm eff}(E_0,a,\theta_i,\theta_o)}\, e^{-x/\lambda_{\rm eff}(E_0,a,\theta_i,\theta_o)} e^{-x/L}. \tag{29}$$

In the limit of $L\gg\lambda$ and $\lambda_{\rm eff}(E_0,a,\theta_i,\theta_o)=\lambda(E_0)$ we obtain the same expression for $K_{\rm sc}$ as in Ref. 9.

Equation (26) allows us to calculate the inelastic electron scattering cross section as determined from a REELS experiment in a general geometry, if the dielectric function $\epsilon(\mathbf{k},\omega)$ of the medium is known. To model the ELF we have used the expansion in Drude-Lindhard type oscillators[10,11,20,21]

$$\mathrm{Im}\left\{\frac{1}{\epsilon(k,\omega)}\right\}=\sum_{i=1}^{n}\frac{A_i\gamma_i\hbar\omega}{(\hbar^2\omega_{0ik}^2-\hbar^2\omega^2)^2+\gamma_i^2\hbar^2\omega^2} \times\theta(\hbar\omega-E_g), \tag{30}$$

with

$$\hbar\omega_{0ik}=\hbar\omega_{0i}+\alpha_i\frac{\hbar^2k^2}{2m}. \tag{31}$$

Here A_i, γ_i, and ω_{0ik} are the oscillator strength, width, and energy position of the ith oscillator. The dependence of ω_{0ik} on k is in general unknown, but Eq. (31) is generally accepted with α_i as an adjustable parameter. The step function $\theta(\hbar\omega-E_g)$ is included to describe the effect of an energy band gap E_g in semiconductors and insulators so that $\theta(\hbar\omega-E_g)=0$ if $\hbar\omega<E_g$ and $\theta=1$ if $\hbar\omega>E_g$. For metals $E_g=0$. We have decided to parametrize the ELF instead of ϵ because the functional shape given to the ELF is closely related with the features appearing in the experimental loss spectra. Besides, it allows one to perform analytically a Kramers-Krönig transformation of $\mathrm{Im}\{1/\epsilon\}$ to obtain

$$\mathrm{Re}\left\{\frac{1}{\epsilon(k,\omega)}\right\}=1-\sum_{i=1}^{n}\frac{A_i(\hbar^2\omega_{0ik}^2-\hbar^2\omega^2)}{(\hbar^2\omega_{0ik}^2-\hbar^2\omega^2)^2+\gamma_i^2\hbar^2\omega^2} + \frac{2}{\pi}\int_0^{E_g}\mathrm{Im}\left\{\frac{1}{\epsilon(k,z)}\right\}\frac{z\,dz}{z^2-\omega^2}. \tag{32}$$

From $\mathrm{Im}\{1/\epsilon\}$ and $\mathrm{Re}\{1/\epsilon\}$, the real and imaginary parts of the dielectric function ($\epsilon=\epsilon_1-i\epsilon_2$) are given by

$$\epsilon_1=\frac{\mathrm{Re}\{1/\epsilon\}}{(\mathrm{Re}\{1/\epsilon\})^2+(\mathrm{Im}\{1/\epsilon\})^2},$$

$$\epsilon_2=\frac{\mathrm{Im}\{1/\epsilon\}}{(\mathrm{Re}\{1/\epsilon\})^2+(\mathrm{Im}\{1/\epsilon\})^2}. \tag{33}$$

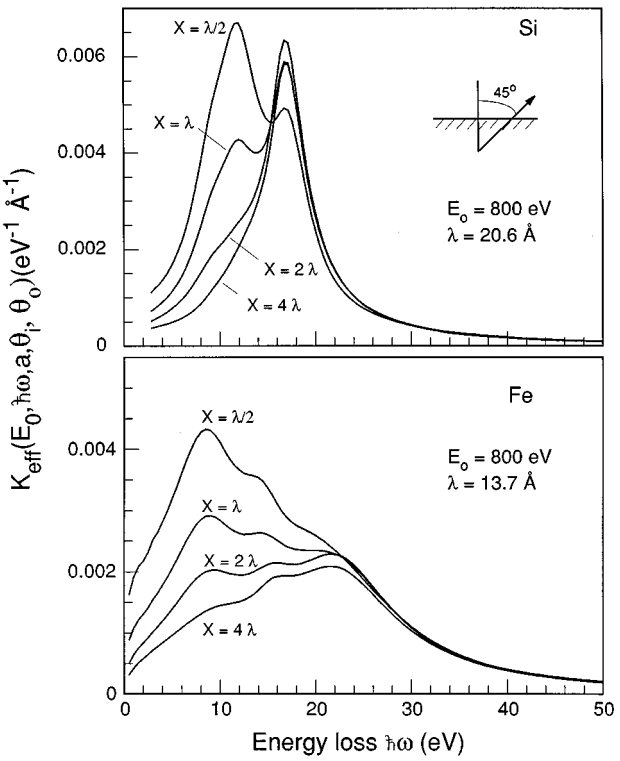

FIG. 3. Path-length dependence of $K_{\rm eff}$ for fixed energy ($E_0=800$ eV) and geometry ($\theta_i=0°$, $\theta_o=45°$) for Si (upper) and Fe (lower). The four path lengths λ/2, λ, 2λ, and 4λ with λ given by the corresponding values for Si and Fe at $E_0=800$ eV [20.6 and 13.7 Å, respectively (Ref. 19)] have been considered.

III. RESULTS AND DISCUSSION

We have made a systematic study of the model for Fe and Si. The ELF for Si and Fe were taken from Ref. 10 and Ref. 20, respectively. The aim of this section is to show the trends followed by $K_{\rm eff}$ and $K_{\rm sc}$ within this formalism as the variables involved $(E_0,\hbar\omega,\epsilon,a,\theta_i,\theta_o)$ change.

Figure 3 shows the path-length dependence of $K_{\rm eff}(E_0,\hbar\omega,a,\theta_i,\theta_o)$ for fixed energy ($E_0=800$ eV) and geometry ($\theta_i=0°$, $\theta_o=45°$) for Si (upper) and Fe (lower). Four different path lengths x have been chosen corresponding to λ/2, λ, 2λ, and 4λ where λ=20.6 Å for Si and 13.7 Å for Fe have been taken from the literature.[19]

For Si, the surface and bulk plasmons are clearly identified as the features at ~11 and ~17 eV, respectively. It is observed that, as expected, the surface plasmon is attenuated as the total path length increases. For Fe the effect is similar with the attenuation of the feature at ~8 eV, which is mainly related with the surface losses.[9]

For $\theta_i=\theta_o=0°$, pronounced oscillations that vary with the path are observed for $K_{\rm eff}$.[9] This is due to the interference of the field set up by the incoming electron on the outgoing electron. When the incidence and exit angles differ from zero, the overlap between the two trajectories decreases and correspondingly these oscillations disappear. This is consistent with the results in Fig. 3 (compare Fig. 3 of this work with Fig. 6 of Ref. 9 for the case of Fe and Fig. 6 from Ref. 10 for Si).

Figure 4 shows the geometry dependence of

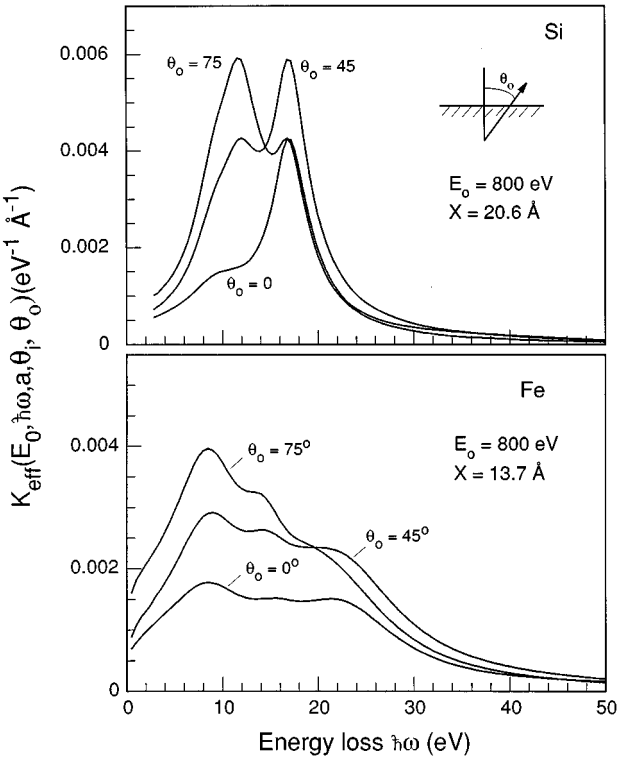

FIG. 4. Geometry dependence of K_{eff} for fixed primary energy of the electrons $E_0=800$ eV and path length $x=20.6$ Å for Si (upper) and $x=13.7$ Å for Fe (lower). Three geometries are considered with a fixed angle of incidence $\theta_i=0°$ and the exit angles $\theta_o=0°$, 45°, and 75°.

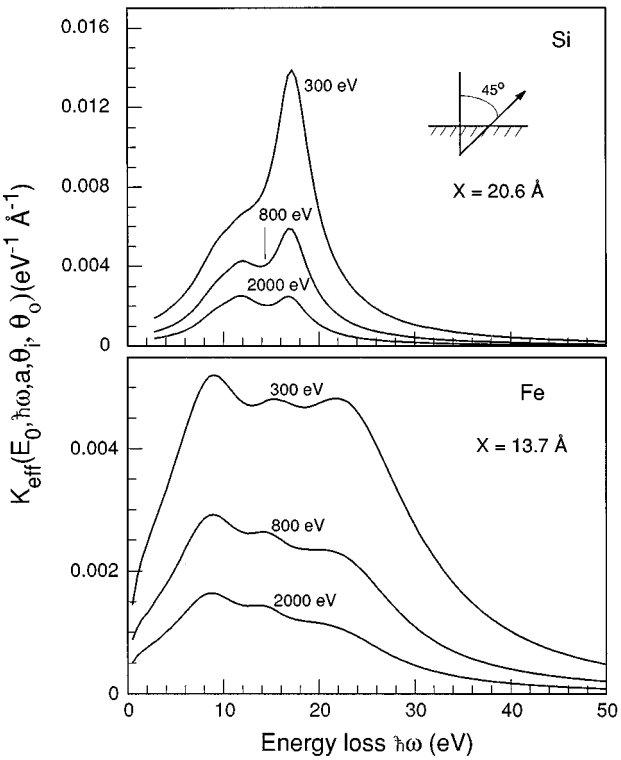

FIG. 5. Energy dependence of K_{eff} for fixed path length (x) and geometry ($\theta_i=0°$, $\theta_o=45°$) for Si (upper) and Fe (lower). Three energies ($E_0=300$, 800, and 2000 eV) are considered. The path lengths $x=13.7$ Å for Fe and $x=20.6$ Å for Si are used.

$K_{\text{eff}}(E_0,\hbar\omega,a,\theta_i\theta_o)$ for fixed primary energy of the electrons $E_0=800$ eV and path length $x=\lambda$, for Si (upper) and Fe (lower). For fixed angle of incidence $\theta_i=0°$ three exit angles $\theta_o=0°$, 45°, and 75° are considered. For glancing exit angles the surface losses are enhanced with respect to the bulk losses as expected. Note that although the path length traveled by the electron inside the solid is the same for all angles, the area increases and by that the effective inelastic mean free path as defined in Eq. (28) decreases with increasing exit angle. This is due to the increased time of interaction of the electron with the solid after it has escaped.

Figure 5 shows the energy dependence of $K_{\text{eff}}(E_0,\hbar\omega,a,\theta_i,\theta_o)$ for fixed path length $x=\lambda$ and geometry ($\theta_i=0°$, $\theta_o=45°$) for Si (upper) and Fe (lower). Three energies ($E_0=300$, 800, and 2000 eV) are considered.

The expected overall attenuation of K_{eff} as E_0 increases is observed. However, an effect that is not obvious is the following: in Fig. 5, the relative contribution of the surface losses with respect to the bulk losses is enhanced at higher primary energies. This happens for both materials, but it is more clearly seen for Si, which has a pronounced surface plasmon peak. Normally one might expect the relative surface excitations to be highest for the lowest primary energies. The explanation is given by the fact that the physical extension of the surface excitations is roughly[2] v/ω_p where v is the velocity of the electron and $\hbar\omega_p$ is the bulk plasmon energy. Then, the region active to surface excitations is proportional to the square root of the primary energy of the electrons. This means that, if we consider a fixed path for the electron trajectory, the ''size'' of the surface region will increase with the primary energy of the electrons. In our case, the active surface region for electrons of 2000 eV is a factor 2.6 larger than for electrons of 300 eV. This is approximately the enhancement of the surface plasmon with respect to the bulk plasmon for these same energies for Si in Fig. 5. The same effect must be observed in a transmission experiment as the primary electron energy is changed, as predicted by Ritchie.[2]

In Fig. 6, the energy dependence of $K_{\text{sc}}(E_0,\hbar\omega,\theta_i,\theta_o)$ [Eq. (26)] for fixed geometry ($\theta_i=0°$, $\theta_o=45°$) for Si (upper) and Fe (lower) is shown. Three energies ($E_0=300$, 800, and 2000 eV) are considered. The same overall attenuation of K_{ac} when E_0 increases is observed as in Fig. 5. The expected relative attenuation of the surface losses with respect to the bulk losses for increasing primary electron energy is observed. This is because electrons with short path lengths have a relatively higher weight [Eqs. (26) and (29)].

Figure 7 shows the geometry dependence of $K_{\text{sc}}(E_0,\hbar\omega,\theta_i,\theta_o)$ for fixed primary energy $E_0=800$ eV for Si (upper) and Fe (lower). Three geometries are considered with fixed incidence $\theta_i=0°$ and exit angles $\theta_0=0°$, 45°, and 75°. As we consider more glancing exit angles the surface losses are enhanced with respect to the bulk losses as expected. Note that the area increases and by that the inelastic mean free path decreases with increasing exit angle. This is, as above, due to the increased time of interaction of the electron with the solid after it has escaped.

In the following paper[22] the validity of the model presented here has been tested experimentally.

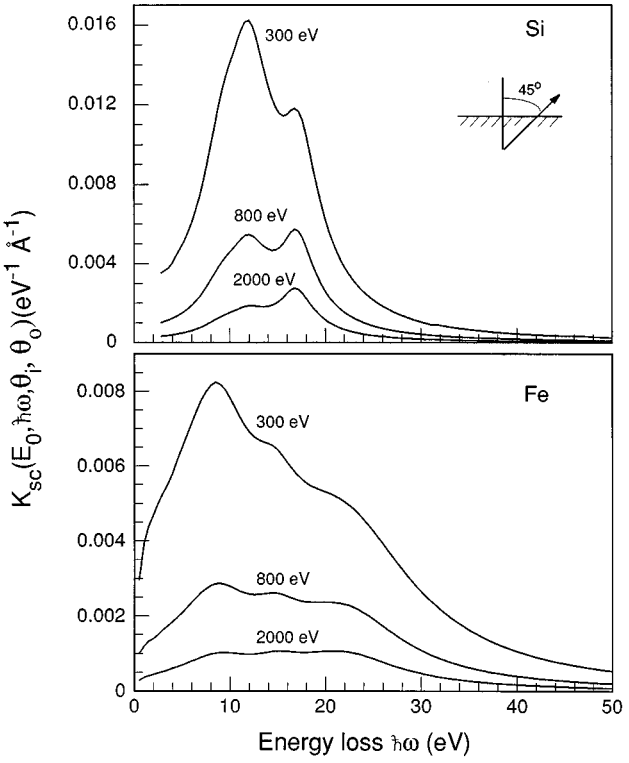

FIG. 6. Energy dependence of K_{sc} for fixed geometry (θ_i=0°, θ_o=45°) for Si (upper) and Fe (lower). Three energies (E_0=300, 800, and 2000 eV) are considered.

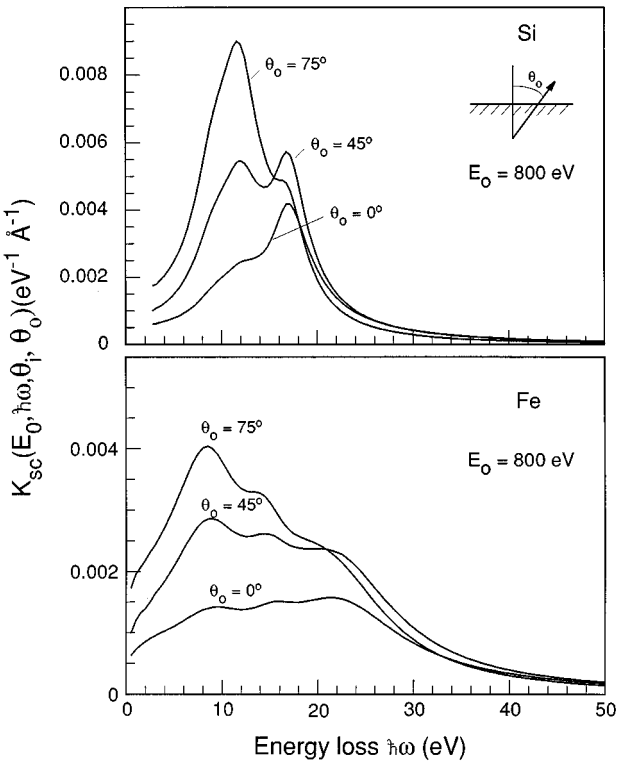

FIG. 7. Geometry dependence of K_{sc} for fixed primary energy of the electrons E_0=800 eV for Si (upper) and Fe (lower). Three geometries are considered with fixed angle of incidence θ_i=0° and the exit angles θ_o=0°, 45°, and 75°.

IV. CONCLUSIONS

A model to calculate inelastic electron scattering cross sections for electrons traveling in a general reflection geometry is proposed. It is based in the so-called surface reflection model. Within the formalism developed in this paper, for a given geometry and energy of the primary electrons, the dielectric function of the sample is the only input for the calculations of the cross section as determined from analysis REELS experiments. A systematic study of the behavior of the model is presented for the case of Si and Fe. Features related with surface losses are, as expected, enhanced at lower primary energies and glancing angles.

For a given trajectory the effective inelastic scattering cross section is almost symmetrical with respect to the interchange of the incidence and exit angles. Besides, the ratio of surface to bulk losses is enhanced for increasing primary electron energies because the physical extension of the region where surface losses can take place increases with the primary electron energy.

The formalism is promising for prediction of the inelastic scattering cross section for electrons backscattered from the surface of solids.

[1] J. Lindhard, K. Dan. Vindesk. Selsk. Mat. Fys. Medd. **28**, 8 (1954).
[2] R. H. Ritchie, Phys. Rev. **106**, 874 (1957).
[3] E. A. Stern and R. A. Ferrel, Phys. Rev. **120**, 130 (1960); A. Otto, Phys. Status Solidi **22**, 401 (1967).
[4] R. F. Egerton, *Electron Energy Loss Spectroscopy in the Electron Microscope* (Plenum, New York, 1986).
[5] H. Raether, in *Excitation of Plasmon and Interband Transitions by Electrons*, edited by G. Höhler, Springer Tracts in Modern Physics Vol. 88 (Springer, New York, 1980).
[6] G. Chiarello, E. Colavita, M. De Crescenzi, and S. Nannarone, Phys. Rev. B **29**, 4878 (1984); Y. Ohno, Phys. Rev. B **39**, 8209 (1989); J. C. Ingram, K. W. Nebesny, and J. E. Pemberton, Appl. Surf. Sci. **44**, 279 (1990); F. Yubero, J. M. Sanz, E. Elizalde, and L. Galán, Surf. Sci. **237**, 173 (1990).
[7] F. Yubero and S. Tougaard, Surf. Interf. Anal. **19**, 269 (1992).
[8] C. J. Tung, Y. F. Chen, C. M. Kwei, and T. L. Chou, Phys. Rev. B **49**, 16 684 (1994).
[9] F. Yubero and S. Tougaard, Phys. Rev. B **46**, 2486 (1992).
[10] F. Yubero, S. Tougaard, E. Elizalde, and J. M. Sanz, Surf. Interface Anal. **20**, 719 (1993).
[11] F. Yubero, J. M. Sanz, J. F. Trigo, E. Elizalde, and S. Tougaard, Surf. Interface Anal. **22**, 124 (1994).
[12] R. H. Ritchie and A. L. Marusak, Surf. Sci. **4**, 234 (1966).
[13] J. L. Gervasoni and N. R. Arista, Surf. Sci. **260**, 329 (1992).
[14] J. Heinrichs, Phys. Rev. B **8**, 1346 (1973); F. Flores and F.

García-Moliner, J. Phys. C **12**, 907 (1979); P. M. Echenique, R. H. Ritchie, N. Barberán, and J. Inkson, Phys. Rev. B **23**, 6486 (1981).
[15] S. Tougaard and I. Chorkendorff, Phys. Rev. B **35**, 6570 (1987).
[16] M. E. Riley, C. J. MacCallum, and F. Biggs, At. Data Nucl. Data Tables **15**, 443 (1975); **28**, 379 (1983).
[17] I. Pazsit and R. Chakarova, Phys. Rev. B **50**, 13 953 (1994).
[18] D. R. Penn, J. Electron Spectrosc. Relat. Phenom. **9**, 29 (1976).
[19] S. Tanuma, C. J. Powell, and D. R. Penn, Surf. Interface Anal. **17**, 911 (1991).
[20] S. Tougaard and J. Kraaer, Phys. Rev. B **43**, 1651 (1991).
[21] R. H. Ritchie and A. Howie, Philos. Mag. **36**, 463 (1977).
[22] F. Yubero, D. Fujita, B. Ramskov, and S. Tougaard, following paper, Phys. Rev. B **53**, 9728 (1996).